

TIME-DEPENDENT COEFFICIENT OF THERMAL EXPANSION OF AN ALKALI-SENSITIVE ROCK IN ALKALINE SOLUTION

Oliver Mielich^{1*}, Hans W. Reinhardt²

¹ Materials Testing Institute University of Stuttgart, Otto-Graf-Institute, GERMANY

² Department of Construction Materials, University of Stuttgart, GERMANY

Abstract

It is well-known that temperature gradients can lead to eigenstresses the concrete. With large temperature differences between the coefficients of thermal expansion of concrete constituents cement stone and aggregate, the calculated stresses are in the range of the tensile strength of concrete. So far, it is assumed that the thermal expansions of alkali-sensitive aggregates are largely independent of the alkaline environment. This paper shows that not only the mechanical properties but also the coefficient of thermal expansion depends on the alkaline medium. What theoretical damage processes may arise during an alkali-silica reaction is, among other things, discussed in this paper.

Keywords: alkali-sensitive rock, coefficient of linear thermal expansion, alkaline solution

1 INTRODUCTION

The alkali-silica reaction (ASR) is one of the biggest problems for the durability of concrete [1]. Basically, ASR concerns a chemical reaction in the concrete between the highly alkaline ($\text{pH} \geq 13.5$) pore solution (OH^- , Na^+ , K^+ , Ca^{2+} -ions), certain SiO_2 modifications of aggregates and water. The SiO_2 needs a critical amount, variety, and distribution to be present. In this case, alkali-silica gels swell upon exposure to water, thereby causing strain and eventually cracks in the concrete. An ASR starts out always by the rock grains, wherein between fast and slow-reacting rocks must be distinguished. For fast-reacting rocks the ASR always starts from the surface of a grain, while in contrast, the ASR for slow-reacting rocks always emanates from the interior of a grain.

The examinations of concrete thin sections show often that a pronounced formation of cracks along grain boundaries inside a grain is presented as characteristic feature. In addition, it can be seen at the grain boundaries that a partial dissolution of the crystal takes place. The cracks in the grain extend into cracks in the cement matrix. The ASR gel is usually found in the cracks of the cement matrix, the adjacent air pores and not in the grain itself [2]. In addition, there seems to be also quartzites, in which the grain boundaries are dissolved within a rock grain, but the crack in the rock does not cause any crack formation in the surrounding cement matrix [2].

Numerical studies can outline the possible causes of injury due to different strain. However, in particular, the input parameters in the numerical calculation are critical. To simulate the crack formation and propagation in concrete, non-linear elastic fracture mechanics is used. For the damage process at micro level especially the works [3, 4, 5, 6] are to be named. In all models is not yet considered that solvents attacks lead to SiO_2 modifications and to softening of the aggregate [7, 8]. In aggregates, which often have a very diverse mineral composition differences in the thermal expansion of individual minerals can lead to stress concentrations at the grain boundaries and contact points. This would result in cracks that occur prior to the formation of the alkali-silica gel. To what extent the alkaline medium changes the coefficient of thermal expansion of alkali-sensitive aggregates and which influence results in damage process at the end of ASR, is one of the open scientific matters.

2 MATERIALS AND METHODS

2.1 Rock used

Quartz porphyry from a quarry in the middle of Germany was selected for the experiments. The mineral composition has been determined by X-ray diffraction. The results are given in Table 1. The alkali sensitivity of the rock was assessed with the accelerated mortar test according to [9] which is derived from [10] and [11]. With the mentioned test quartz porphyry was found to be ASR sensitive [2]. From a large boulder cores were drilled out for the investigations of mechanical properties

* Correspondence to: oliver.mielich@mpa.uni-stuttgart.de

[2, 7, 8]. From a larger drill core were, to determine the thermal expansion, further cylindrical specimen (diameter of 9.4 mm and a length of approx. 25 mm) worked out (Fig. 1).

2.2 Exposure conditions

As synthetic pore solutions a 0.1 molar (pH = 13) and a 1.0 molar (pH = 14) potassium hydroxide solution (KOH solution) were used. With the pore solution used conditions should be created which correspond in terms of pH and main ion type (K^+), determined as K_2O , to a Portland cement pore solution.

Four cylindrical specimens were upright stored in sealed wide mouth bottles with KOH solution and to the relevant test date in a drying oven at $(40.0 \pm 2.0)^\circ\text{C}$ and $(80.0 \pm 2.0)^\circ\text{C}$. On three test specimens, the thermal expansion should be determined, one specimen should be used for light microscopic investigations. The KOH solution was filled so that the samples were 10 mm below the surface and thus fully immersed in the KOH solution. For test date after 30, 60 and 90 days of storage the samples were removed from the KOH solution, rinsed with distilled water and dried for at least 24 hours in a desiccator. Following the measurement of the thermal expansion, the cylindrical specimens were given back in the wide-mouth bottles and the KOH solution was renewed. Table 2 gives an overview of the inspection dates and the storage conditions. (The designation of specimen in the following is i.e. 30_0.1_80: the first number gives the storage duration, the second number the concentration of the KOH solution and the third number the exposure temperature).

2.3 Testing method

As a device for electronic measurement of linear thermal expansion, the thermo-mechanical Analyzer TMA 402 F3 Hyperion Netzsch with an inductive displacement sensor was available. The technology of the analyzer enables measurements of the smallest length changes in the nanometer range (digital resolution 0.125 nm). A great advantage when measuring compared to [12] is that the entire measuring system is thermally stabilized via water-cooling. In this way, influencing the measurement is inhibited by introduction of heat from the furnace or fluctuating ambient temperatures. All connections are vacuum-tight designed so that measurements in a highly pure atmosphere or vacuum are possible.

The thermal expansion was determined in the temperature range of $+20$ to $+80^\circ\text{C}$. Based on the room temperature was maintained at $(20 \pm 0.2)^\circ\text{C}$, this held over 2 h and the off-path length (l_{s20}) determined the specimen. It was then approached at a rate of $0.5^\circ\text{C}/\text{min}$ a temperature of $(80 \pm 0.2)^\circ\text{C}$ min, this held over 2 h and determine the final length of the specimen (l_{s80}). To evaluate the residual elongation length, the measured values were taken at 20°C and 80°C (l_{s20} and l_{s80}) at the end of the hold time points. As calibrated reference sample, an aluminum oxide sample was used with known thermal expansion in the temperature range from 20°C to 80°C .

2.4 Microscopic examinations

According to the experiences of [2] thin sections were prepared for studies with optical polarizing microscope. For 30, 60 and 90-day storage, of a cylindrical sample were cut off a slices taken. From the slices, uncovered polished thin section samples were prepared with pore space coloring on a glass slide. The pore space coloring was done with a blue colored epoxy resin (colored with Oracet blue epoxy resin) by vacuum impregnation. By means of polarization microscope Orthoplan pole of Leitz thin sections were studied.

3 RESULTS

Linear thermal expansion

From three cylindrical specimens of each combination (Tab. 2) the standard deviation and coefficient of variation of the coefficient of thermal expansion was determined. In Fig. 2 the test scatter after 30 days of storage of combinations 30_0.1_40, 30_1.0_40 and 30_0.1_80 are within the test scatter of the zero sample (initial state). The results of the combination 30_1.0_80 is outside the scatter of the zero sample and the other combinations. The coefficients of variation are in a range of 3.5 to 8.5%.

Comparing with the results after 30 days of storage are the scatter of the first three combinations after 60 days of storage within the scatter of the zero sample (Fig. 3). Outside the scatter is just the combination 60_1.0_80. The coefficients of variation are in a range of max. 10%.

Fig. 4 shows that the average values of coefficients of thermal expansion after 90 days of storage in the sequence 90_0.1_40 – 90_0.1_80 – 90_1.0_40 – 90_1.0_80. The scatter of combinations 90_1.0_40 and 90_1.0_80 are outside the scatter of the zero sample. The coefficients of variation are in a range of 0.8 to 7.5%.

In Tab. 3 the length increases are given as mean values, arising after 60 and 90 days storage in the KOH solutions. The length increases were calculated as the difference of the initial length l_{s20} of the test specimens after 60 and 30 days storage, as well as the difference between the initial length of the test specimens l_{s20} after 90 and 30 days. It is found in all storage combinations that the specimen length increases with increasing storage time.

Microscopic examination of thin sections

From each combination a thin section was prepared and analyzed by polarization microscopy on a cylindrical specimen at the end of each storage. Fig. 5 shows that the degree of dissolution and disintegration after 90 days of storage at the combination 90_1.0_80 is greatest. The dissolution and disintegration range up to 2 mm into the specimen. In the center of the specimen was the fine-grained matrix, as in the zero sample (initial state), completely intact. In contrast 90_1.0_40 dissolution and disintegration were detected mainly near the surface in the combinations 90_0.1_40, 90_0.1_80. The dissolution of the typical fine-grained quartz porphyry matrix leads to an increase in the porosity of the structure, which is confirmed by the presence of blue-tinted impregnating resin in the structure. The increased porosity in the peripheral region also represents a preferred passage means for further penetration of the KOH solution.

4 DISCUSSION

General

The determined coefficient of thermal expansion of zero sample is in the range from customary quartz porphyries of $4.1E-6$ to $8.3E-6$ 1/K [13]. The scatter achieved are not unusual for material testing when determining the coefficient of thermal expansion with coefficient of variation of max. 10%.

Effect of heating rates

Heating rates of not more than $2^{\circ}\text{C}/\text{min}$ are necessary to eliminate the formation of cracks due to stress generated by thermal gradients in samples with a diameter of 6 mm [14] for the precise measurement of the temperature expansion. It can therefore be assumed that the chosen heating rate of $0.5^{\circ}\text{C}/\text{min}$ leads to a significant reduction of newly formed cracks by thermally induced stresses.

Effect of microcracks in pristine rocks

The authors [15] and [16] have shown that the average thermal expansion of rocks with a large number of microcracks is less than the mean thermal expansion of the individual crystals. The formation of microcracks in a rock by mechanical, external influence leads to reduction of the coefficient of thermal expansion of same rock without mechanical, external influence. Cracks in the crystals themselves and along grain boundaries allow for thermal expansion of the existing pore space without contributing to the overall expansion of the rock [14]. Existing cracks before the heating and cooling thus do not contribute to a possible residual elongation at room temperature.

In the formation of microcracks can be distinguished, whether they are natural or artificially induced. Artificially induced microcracks caused by blasting operations, core withdrawals so-as evidenced by the preparation of aggregates by jaw crusher, ball crusher and others. Recent studies on a granodiorite showed [17] that a significant influence on the type of process ASR due to the formation of different micro-cracks or micro crack patterns in the rock grain under external alkali supply is not detectable. In addition to the external stresses, internal thermal stresses affect the cracking and crack propagation, which causing structural intergranular tensions due to the different thermal expansion behavior of-rock-forming minerals. Open in-situ microcracks have a preferred orientation and therefore a significant influence on physical-mechanical rock properties.

Effect of exposure on physical and mechanical properties of rock

The experiments demonstrate (Table 4) that depending on storage time, alkaline environment and temperature a reduction of the coefficient of thermal expansion, as a physical rock property, occurs.

Results from mechanical properties of quartz porphyry are reported by Reinhardt and Mielich [7]. They measured a reduction of the modulus of elasticity in the range of 10 to 41% after 70 and 140 days storage in a 40°C warm 1.0 molar KOH solution. Table 4 shows that the coefficient of thermal expansion of identical quartz porphyry after 90 days exposure in the 40°C warm 1.0 molar KOH solution (90_1.0_40) is reduced by 12%. It is therefore assumed that when stored more than 90 days, the coefficient of temperature expansion will continue to decline.

Independent from the source, the solubility and mobilization of rock minerals, which depends strongly on a high concentration of OH⁻, leads to a reduction of mechanical rock properties [7]. This is consistent with the work of Copuroglu et al. [18], who studied three types of rock in warm alkaline solution and found a reduction of the elastic modulus which was supposedly due to silica dissolution. The work of Ben Haha [19] showed that alkaline solution leads to a reduction of fracture energy and the brittleness of reactive rocks.

Summarized it can be noted that alkali-sensitive rocks are unstable in high alkaline environment and undergo an alteration. This deterioration feature of alkali-sensitive rocks is irreversible and affects mechanical and physical properties of rock or aggregate and influence indirectly the integrity of concrete.

Effect of dissolution processes

The determination of the residual strain after cooling is an indicator of the degree of structural damage in the rock. In contrast, discontinuous measurements of the initial length of one and the same specimens before heating at room temperature (l_{s20}) are an advantage in capturing the increase in length by dissolving operations in the rock. The light-microscopic studies (Fig. 5) have shown that the SiO₂ dissolution process and other rock-forming minerals originating from the marginal zone of the surface of the alkali-sensitive quartz porphyry. At least the SiO₂ dissolution process seems to be participating in the increase in length of the test specimens (Tab. 3). Transferred to ASR sensitive concrete, it would mean that increase take place before gel formation. Similar results are reported by Garcia-Diaz et al. [20]. The authors suppose an increase in volume and a related material pressure build-up alone as a result of the SiO₂ dissolution process even before the actual gelation. A combination with the results of [2, 21] would also explain why is expected a decrease of strength and deformation properties before a measurable increase in strain appears (Fig. 6).

Effect on concrete tests

In concrete prism or ASR performance tests, prior to any length change measurements prisms must be cooled down in case of discontinuous measurements, however, without defined cooling rate. This procedure produces both humidity and temperature gradient, which leads to internal stresses [22] in the specimen. To make matters worse, the thermal expansion of the aggregate and the formation of additional cracks inside a grain may be the result of the influence of the SiO₂ dissolution process and other rock-forming minerals as mentioned above. Eventually, an additional cracking would have a remaining, residual strain irreversible consequence that would distort the assessment criterion elongation as well as the characteristic features of the ASR falsified. This would also explain that cracks along grain boundaries inside a grain can be found, but not an ASR gel itself. This is usually found in the cracks of the cement paste and in the adjacent air pores.

5 CONCLUSIONS

The paper has reported on experimental and theoretical investigations with one alkali-sensitive rock. The alkali-sensitive rock was quartz porphyry. The time-dependent coefficient of thermal expansion was measured after exposure in pore solutions, which differ in their temperature and concentration. The main conclusions are:

- i) Alkali-sensitive rocks are unstable in high alkaline environment and undergo an alteration. This deterioration feature of alkali-sensitive rocks is irreversible and affects physical and mechanical properties of rock or aggregate and influence indirectly the integrity of concrete.
- ii) The determination of the initial length (l_{s20}) after 30, 60, and 90 days exposure appears to be an indicator for SiO₂ release.
- iii) The increase in length after exposure in synthetic pore solution depends only slightly on the concentration of solution. This requires further investigations.
- iv) Transferred to ASR sensitive concrete, it would mean that expansion take place before gel formation. This could mean that the current test procedures have to be reconsidered.
- v) Further investigations are necessary to better understand the damage and cracking processes in a rock grain. The choice of temperature, heating and cooling rates and concentration of external alkali supply in accelerated test procedures and performance tests must be systematically scrutinized. One has to make sure that the aggregates are not rejected due to negative testing influences.
- vi) A larger data base of physical-mechanical characteristic would help to create a realistic model of ASR damage processes especially on the micro level.

6 REFERENCES

- [1] Rajabipour, F, Giannini, E, Dunant, C., Ideker, J.H., Thomas, MDA (2015): Alkali-silica reaction: Current understanding of the reaction mechanisms and the knowledge gaps. *Cement and Concrete Res.* 76: 130-146.
- [2] Mielich, O. (2010): Contribution to the damage mechanisms in concrete with slow-reacting alkali sensitive aggregates. DAFStb bulletin 583, Berlin, 2010 (in German)
- [3] Dunant, C.F., Scrivener, K.L. (2010): Micro-mechanical modelling of alkali-silica reaction induced degradation using AMIE framework. *Cement and Concrete Res.* 40: 517-525.
- [4] Dunant, C.F., Scrivener, K.L. (2012): Effects of uniaxial stress on alkali-silica reaction induced expansion of concrete. *Cement and Concrete Res.* 42: 567-576.
- [5] Dunant, C.F., Scrivener, K.L. (2012): Effects of aggregate size on alkali-silica reaction induced expansion. *Cement and Concrete Res.* 42: 745-751.
- [6] Giorla, A.B., Scrivener, K.L., Dunant, C.F. (2015): Influence of visco-elasticity on the stress development induced by alkali-silica reaction. *Cement and Concrete Res.* 70: 1-8.
- [7] Reinhardt, H.W., Mielich, O. (2014): Fracture toughness of alkali-sensitive rocks in alkaline solution. *International Journal of Rock Mechanics & Mining Sciences* 70: 552-558.
- [8] Reinhardt, H.W., Mielich, O. (2011): A fracture mechanics approach to the crack formation in alkali-sensitive grains. *Cement and Concrete Res.* 41: 255-262.
- [9] Franke, L, Witt, S. (2004): Accelerated test for alkali reaction: application of an internationally recognized quick test to German conditions. *Concrete Plant + Precast Technology* 70, No. 5: 14-21.
- [10] Oberholster, R.E., Davies, G. (1986): An accelerated method for testing the potential alkali reactivity of siliceous aggregates. *Cem. Concr. Res.* 16, No. 2: 181-189.
- [11] RILEM Recommended Test Method AAR-2 (2000): Detection of Potential Alkali-Reactivity of Aggregates. The Ultra accelerated Mortar-bar Test. *Materials and Structures* 33, No. 229: 283-289
- [12] German Institute for Standardization: DIN EN 14581 - Natural stone test methods - determination of the linear thermal expansion coefficient. German version EN 14581: 2004, March 2005 issue
- [13] Dettling, H. (1962): The thermal expansion of the cement stone, the rocks and concretes. Otto Graf Institute, Governmental Research and Material Testing Institute for Civil Engineering, Technical University of Stuttgart, (in German)
- [14] Judge, D., Simmons, G. (1977): Thermal expansion behavior of igneous rocks. *Int. J. Rock. Mech. Min. Sci. & Geomech., Abstr.* Vol 11, (1977): 403-411.
- [15] Baldrige, W.S., Miller, F., Wang, H., Simmons, G. (1972): Thermal expansion of Apollo lunar samples and Fairfax diabase. *Proc. 3rd Lunar Sci. Conf.* 3.
- [16] Todd, T., Richter, D., Simmons, G., Wang, H. (1973): Unique characterization of lunar samples by physical properties. *Proc. 4th Lunar Sci. Conf.* 3.
- [17] Giebson, C.; Dietsch, S.; Seyfarth, K.; Ludwig, H.-M. (2015): ASR under combined influence – Processes in aggregate. 19th International Conference on Building Materials, IBAUSIL 2015, Weimar, (in German)
- [18] Copuroglu, O., Schlangen, E., Andic-Cakir, Ö., Garcia-Diaz, E. (2010): Effect of silica dissolution on the mechanical characteristics of alkali-reactive aggregates. *Journal Advanced Concrete Technology* 8 (1): 5-14.
- [19] Ben Haha, M. (2006) : Mechanical effects of alkali silica reaction in concrete studied by sem-image analysis. Ph.D. thesis, Ecole Polytechnique Federale de Lausanne, n°3516
- [20] Garcia-Diaz, E., Riche, J., Bulteel, D., Vernet, C. (2006): Mechanism of damage for the alkali-silica reaction. *Cement and Concrete Res.* 36: 395-400.
- [21] Reinhardt, H.W., Mielich, O. (2012): Mechanical properties of concretes with slowly reacting alkali sensitive aggregates. *Conference Proceedings of the 14th ICAAR, Austin, TX, USA*
- [22] Weise, F, Voland, K., Pirskawetz, S., Meinel, D. (2012): Analysis of ASR-induced damage processes in concrete: Application of innovative measurement techniques. *Beton- und Stahlbetonbau, Volume 107, Issue 12: 805-815*

TABLE 1: Major mineral composition of the rock used.

rock type	mineral composition						
	quartz	feldspar	plagioclase	chlorite	carbonate	mica	kaolinite
quartz porphyry	22.0	33.7	34.5	2.6	1.8	4.6	0.6

TABLE 2: Test dates and storage conditions.

storage times in days	KOH solution in mol/l	temperature in °C
30 – 60 – 90	0.1	40
	0.1	80
	1.0	40
	1.0	80

TABLE 3: Mean values of increase in length after 60 days ($\Delta l_{60d-30d}$) and 90 days ($\Delta l_{90d-30d}$) storage at temperature of 20°C.

	elongation Δl in mm				
	0.1_40	0.1_80	1.0_40	1.0_80	
	$\Delta l_{60d-30d} = \Delta l_{s20,60d} - \Delta l_{s20,30d}$	0.065	0.065	0.053	0.069
	$\Delta l_{90d-60d} = \Delta l_{s20,90d} - \Delta l_{s20,60d}$	1.044	1.035	1.056	1.033
$\Delta l_{90d-30d} = \Delta l_{s20,90d} - \Delta l_{s20,30d}$	1.109	1.100	1.109	1.102	

TABLE 4: Mean values of coefficient of thermal expansion under the effect of concentration and temperature.

storage time	linear coefficient of thermal expansion α in 1/K, (%)			
	0.1_40	0.1_80	1.0_40	1.0_80
0	8.07E-06 (100)			
30	7.69E-06 (95)	7.33E-06 (91)	7.46E-06 (92)	6.09E-06 (75)
60	7.66E-06 (95)	7.41E-06 (92)	7.42E-06 (92)	6.18E-06 (77)
90	7.38E-06 (91)	7.26E-06 (90)	7.13E-06 (88)	4.94E-06 (61)



FIGURE 1: Drill core and specimens (left). Cylindrical specimens between push rod and sample table in the analyzer TMA 402 F3 Hyperion Netzsch (right).

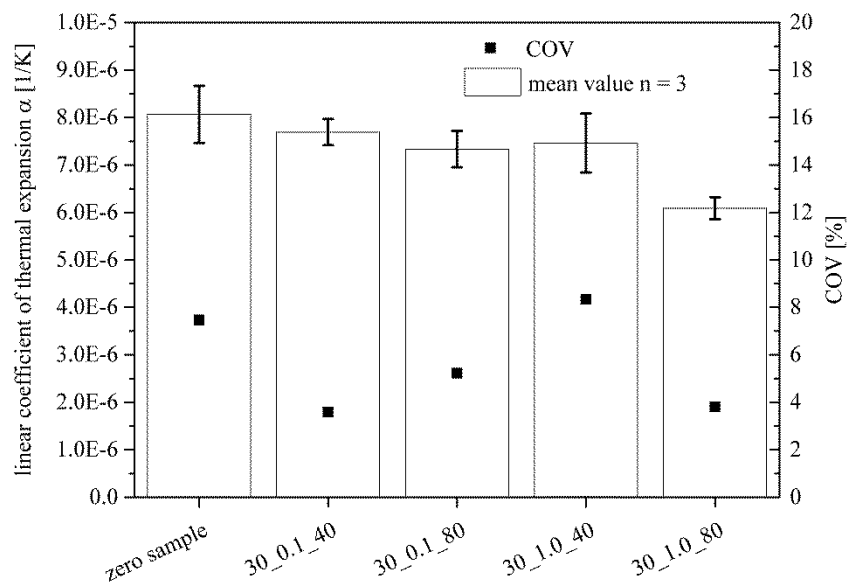


FIGURE 2: Linear coefficient of thermal expansion, scattering range and coefficient of variation (COV) after 30 days storage in 0.1 and 1.0 molar KOH solution at 40°C and 80°C.

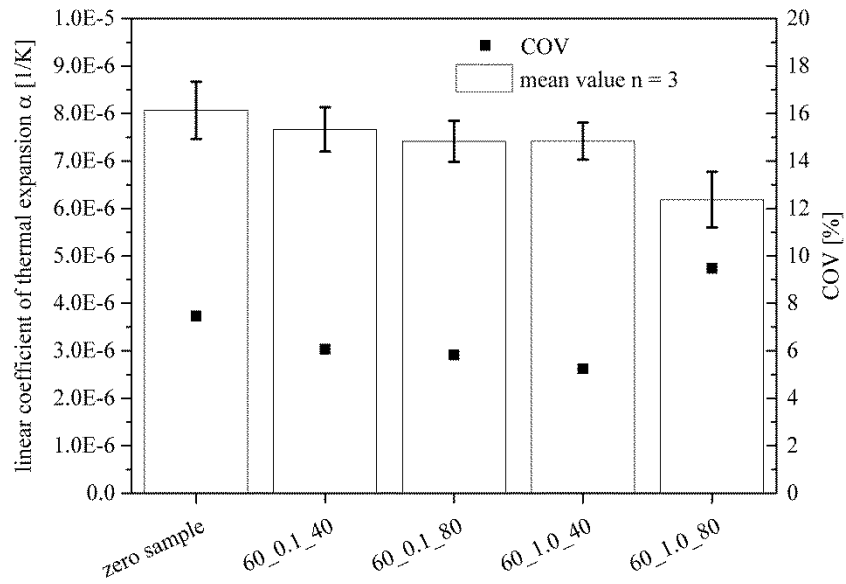


FIGURE 3: Linear coefficient of thermal expansion, scattering range and coefficient of variation (COV) after 60 days of storage in 0.1 and 1.0 molar KOH solution at 40°C and 80°C .

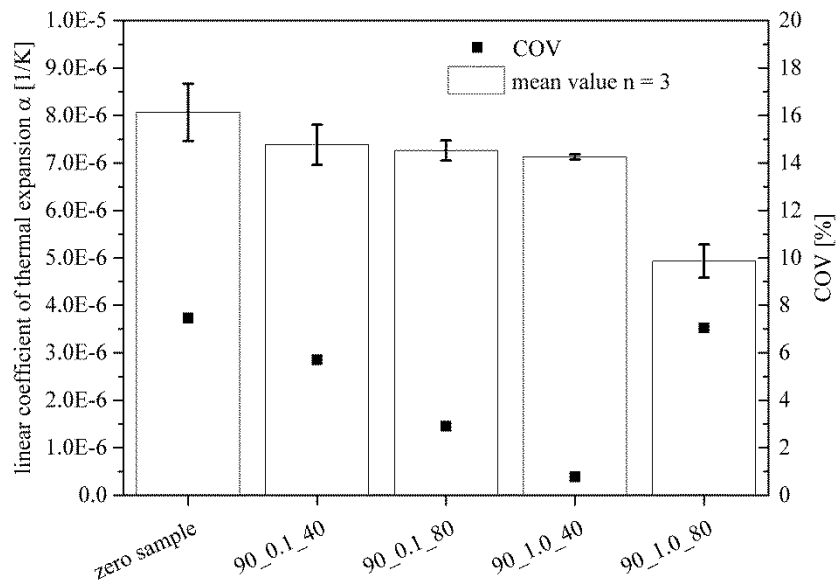


FIGURE 4: Linear coefficient of thermal expansion, scattering range and coefficient of variation (COV) after 90 days of storage in 0.1 and 1.0 molar KOH solution at 40°C and 80°C .

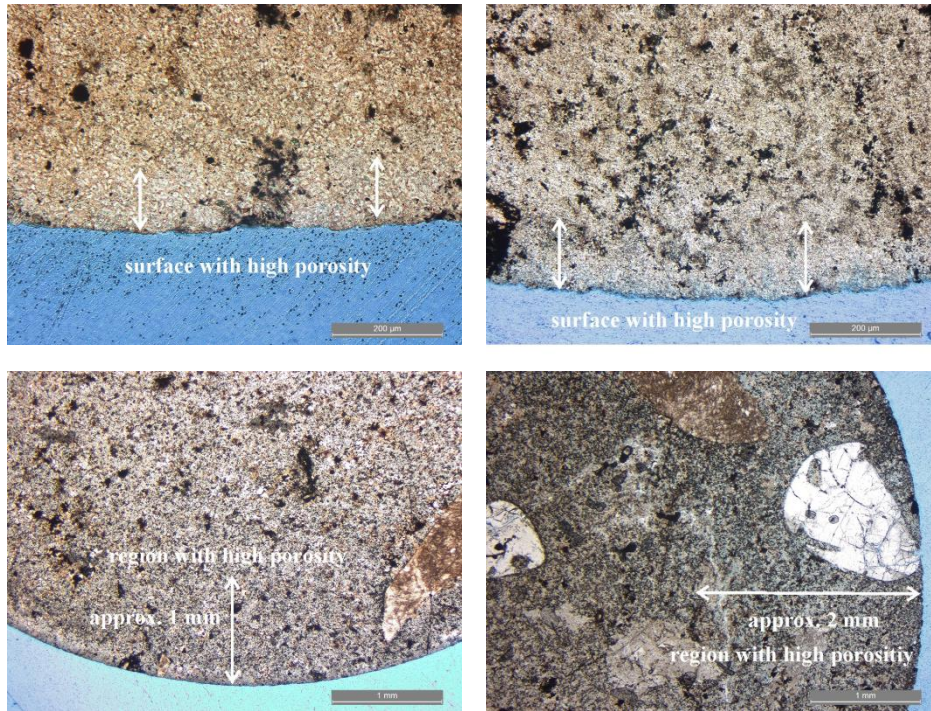


FIGURE 5: Structure of quartz porphyry matrix after 90 days of storage of combinations 90_0.1_40 (top left), 90_0.1_80 (top right), 90_1.0_40 (bottom left) and 90_1.0_80 (bottom right).

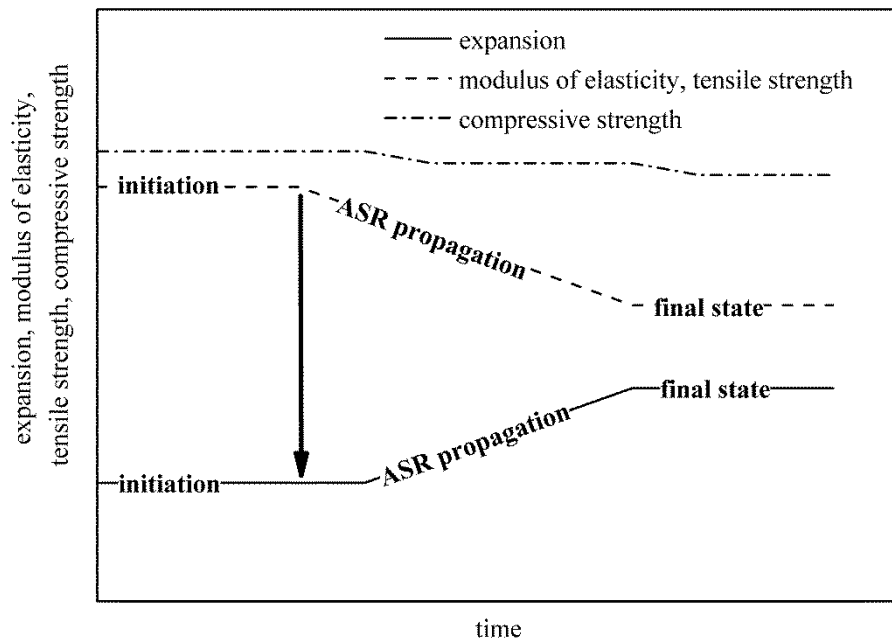


FIGURE 6: Schematic representation of the expansion history and development of the modulus of elasticity, tensile strength and compressive strength of concrete at the expiry of an alkali-silica reaction from the results in [2, 21].